The Astrophysical Journal, 665: L139–L142, 2007 August 20

FAR-ULTRAVIOLET OBSERVATIONS OF THE MONOGEM RING

I.-J. Kim,[1] K.-W. Min,[1] K.-I. Seon,[2,3] J.-W. Park,[1] W. Han,[2] J.-H. Park,[2] U.-W. Nam,[2]
J. Edelstein,[3] R. Sankrit,[3] and E. J. Korpela[3]
Received 2007 June 22; accepted 2007 July 9; published 2007 August 6

ABSTRACT

We present the results of far-ultraviolet (FUV) observations of the Monogem ring made with the FIMS/SPEAR instrument. The global map constructed from the C IV λλ1548, 1550 emission lines presents clear evidence of the interaction of the Monogem ring with the ambient medium. The image shows a half-ring feature in the low-latitude region, with its peak along the distorted boundary of the X-ray ring, where hot gas is in direct contact with the newly found Hα ring (the Gemini Hα ring) centered at (l, b) ~ (191.5°, +5.0°). Only a small portion of the X-ray ring is bright in C IV in the high-latitude region, where hot gas is seen to extend to a great distance from the ring. We have also detected other ionic emission lines in several regions of the Monogem ring, such as C III λ977, O VI λλ1032, 1038, Si II* λ1533, He II λ1640, and O III] λ1666.

Subject headings: ISM: individual (Monogem ring) — ISM: lines and bands — supernova remnants — ultraviolet: ISM

1. INTRODUCTION

Diffuse soft X-ray enhancement in the Monoceros and Gemini constellations was first discovered and examined by observations of rocket flights in the 1970s (Bunner et al. 1971, 1973; Yentis et al. 1972; Davidsen et al. 1972; Long et al. 1977). Later, observations with moderate spatial resolution (1.5°) by *HEAO-1* revealed a more or less limb-brightened shell structure, which was named the "Monogem ring" (Nousek et al. 1981). Detailed studies with *ROSAT* showed that the average temperature was $\log(T/\mathrm{K}) \sim 6.15$ and the neutral hydrogen column density $\sim 5.0 \times 10^{19}$ cm^{-2} (Plucinsky et al. 1996). Based on the observations, Plucinsky et al. (1996) concluded that the Monogem ring is a supernova remnant (SNR) in the adiabatic stage. With an estimated distance of 300 pc, its radius is ~66.5 pc, its age ~86,000 yr, and the initial explosion energy $\sim 1.9 \times 10^{50}$ ergs. The ambient density is extremely low, with a value of $\sim 5.2 \times 10^{-3}$ cm^{-3}. The corresponding thermal pressure of the X-ray emitting gas is $\sim 4.5 \times 10^{4}$ K cm^{-3}, which is only 2–4 times higher than the estimated pressure of the undisturbed interstellar medium (ISM) (Slavin & Cox 1992). As a result, the Monogem ring is expected to arrive at pressure equilibrium with the ISM before it reaches a radiative stage during its evolution. While Plucinsky et al. (1996) contended that the radio pulsar PSR B0656+14, located off the center of the Monogem ring, is not associated with the SNR, because its proper motion is toward the center of the remnant, Thorsett et al. (2003) argued that the center of the remnant only appears displaced because the remnant material is blocked by the Galactic plane and cannot expand significantly in the low-latitude region, whereas it can expand freely in the high-latitude region. If the pulsar and the SNR were born from the same supernova explosion, the distance to the Monogem ring can be more strictly constrained with a parallax distance of ~288 pc to the pulsar, which was estimated by new very long baseline interferometric measurements (Brisken et al. 2003).

The low density of the Monogem ring makes it difficult to detect neutral shells and optical filaments usually seen in supernova remnants when they interact with the ambient interstellar medium (Plucinsky et al. 1996). In fact, there has been no report of clear neutral shells observed in radio wavelengths other than inferences from magnetic field observations reported by Vallée et al. (1984). In the optical domain, there have been only two small faint filaments reported thus far. Reimers & Wendker (1984) observed a thin filament ~1° long in the [O II] line and suggested that it could be a slow shock front (30–50 km s^{-1}) associated with the SNR. Recently, Weinberger et al. (2006) found a ~20′ long, thin (~1′) filament in the Hα and [S II] lines in a region where interaction with the expanding remnant is suspected. If these observations truly indicate interactions of the Monogem ring with the ambient material, it would be interesting to investigate whether any significant features are visible in the far-ultraviolet (FUV) wavelengths, as the SNR is bright in X-ray.

In this Letter, we present the results of FUV observations made for the entire region of the Monogem ring using the Far-Ultraviolet Imaging Spectrograph (FIMS), also known as Spectroscopy of Plasma Emission from Astrophysical Radiation (SPEAR). In particular, we have identified large features in the C IV λλ1548, 1550 emission lines image, which are closely correlated with the region of X-ray enhancement (X-ray ring). The morphology of the C IV map clearly indicates interaction of the hot gas with the ambient medium, manifested in the Hα image.

2. OBSERVATIONS AND DATA REDUCTION

FIMS/SPEAR is designed to observe large-scale diffuse FUV emission lines from the ISM (Edelstein et al. 2006a). FIMS/SPEAR consists of dual FUV imaging spectrographs: the short-wavelength channel (S-channel; 900–1150 Å, 4.0° × 4.6′ field of view) and the long-wavelength channel (L-channel; 1340–1750 Å, 7.4° × 4.3′ field of view), with $\lambda/\Delta\lambda \sim 550$ spectral resolution and 5′ angular resolution. The instrument, its on-orbit performance, and the general procedures of the data analysis are described in detail in Edelstein et al. (2006b).

The Monogem ring was one of the primary program targets and was observed early in the mission, between 2003 December 13 and 2004 January 19. The observation was made by scan-

[1] Korea Advanced Institute of Science and Technology, 305-701, Daejeon, South Korea; ij.kim@kaist.ac.kr.
[2] Korea Astronomy and Space Science Institute, 305-348, Daejeon, South Korea.
[3] Space Sciences Laboratory, University of California, Berkeley, CA 94720.

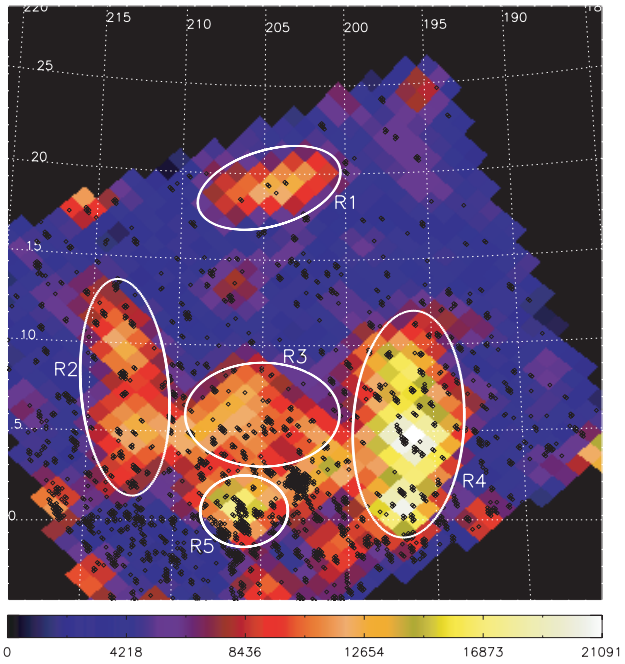

FIG. 1.—FIMS/SPEAR C IV λλ1548, 1550 emission lines image of the Monogem ring in Galactic coordinates. The unit of the color bar annotation is photons s^{-1} cm^{-2} sr^{-1} (LU). The values are not corrected for interstellar extinction. The small diamonds are the pixels masked to remove stellar contamination. Spectra in Fig. 3 are extracted from five subregions designated by R1 through R5.

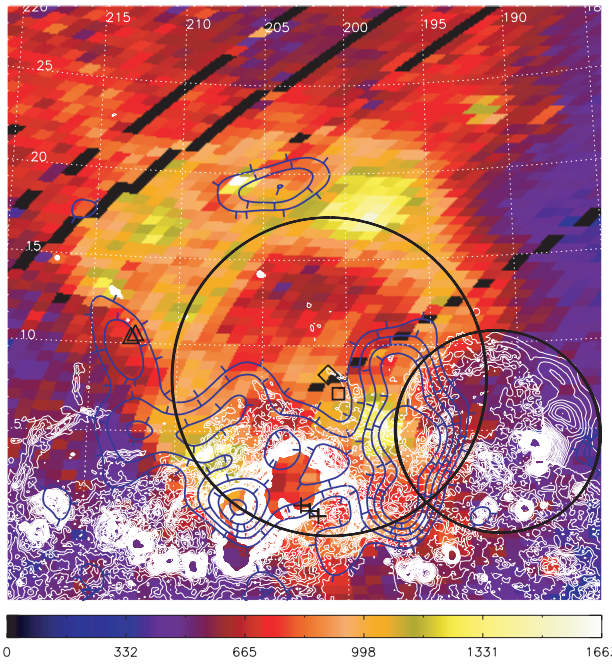

FIG. 2.—FIMS/SPEAR C IV contours and Hα contours overlaid on the RASS X-ray (0.25 keV) image. The unit of the color bar annotation is 10^{-6} counts s^{-1} $arcmin^{-2}$. The C IV contours (*thick blue curves*) are from 8 to 16 × 10^3 LU with 2 × 10^3 LU intervals, and the Hα contours (*thin white curves*) are from 8 to 86 rayleighs with 2 rayleigh intervals. The perpendicular tick marks in the C IV contours represent the downhill direction. The plus signs and triangle symbols indicate the positions of optical filaments reported in Reimers & Wendker (1984) and Weinberger et al. (2006), respectively. The position of pulsar PSR B0656+14 is marked by a diamond with a 9.2° circle centered on this. The estimated position of the pulsar 10^5 yr ago is also marked with a square (Thorsett et al. 2003). The newly found Hα ring (Gemini Hα ring) is indicated by a 5.7° circle centered at (l, b) ~ (191.5°, +5.0°).

ning the Monogem ring region in the direction across the slit of the FIMS/SPEAR instrument. Of the 69 total orbits, 15 orbits were observed by a single sweep, and 54 orbits were observed by multiple sweeps. We have limited our analysis to the region that includes the Monogem ring with $6^h12^m \le \alpha \le 8^h$ and $-3° \le \delta \le +27°$ (J2000.0).

Since our primary concern is the diffuse emission, we removed the data recorded when the count rate was high (>1000 counts s^{-1}), as these events are mostly associated with observation of bright stars. The photons of these bright stars were scattered and spread over the whole field of view, dominating over any diffuse emission that might exist. For the L-channel data, we have selected only the 1360–1680 Å portion for the present analysis, so as to exclude the strong geocoronal airglow line O I λ1356 and the long-wavelength part, which was contaminated by a relatively large detector background. We eventually obtained a total of 3.8 × 10^6 events with an average exposure time of ~29.1 s in the L-channel, and 2.7 × 10^5 events with ~16.9 s average exposure time in the S-channel for the area of present concern. To obtain images and spectra, we have adopted the HEALPix scheme (Górski et al. 2005) with the resolution parameter `Nside` = 512, corresponding to a pixel size of ~6.87′, and 1 and 0.5 Å wavelength bins for the L-channel and the S-channel, respectively. The effects of bright stars were further reduced by masking pixels whose L-channel continuum intensity was higher than 20,000 photons s^{-1} cm^{-2} sr^{-1} $Å^{-1}$ (CU). The median value was ~2714 CU before the removal of these high-intensity pixels.

3. DATA ANALYSIS AND RESULTS

For the C IV emission lines image, we took the 1532–1568 Å portion of the L-channel spectrum and fitted it with a constant continuum plus C IV λλ1548, 1550 lines for each pixel. For better statistics, we increased the pixel size by 8 times (Nside = 64, corresponding to a pixel size of ~55.0′). We assumed a 2 : 1 line ratio for 1548 and 1550 Å doublet lines (Seon et al. 2006). The model spectrum was convolved with a Gaussian function with the width of the FIMS/SPEAR spectral resolution. The image was then smoothed using the spherical version of a Gaussian kernel whose full width at half-maximum (FWHM) was 120.0′ (Seon 2006).

Figure 1 shows the final result of the C IV emission lines image in Galactic coordinates. The small diamonds indicate the positions of the masked pixels. It is seen in the figure that C IV is enhanced only in the low-latitude region, while most of the upper half is missing, with only a small portion remaining in the high-latitude region. We have marked the bright regions with designations R1 through R5, of which R4 is the brightest in the C IV intensity, with its peak value estimated to be ~2.1 × 10^4 photons s^{-1} cm^{-2} sr^{-1} (hereafter LU) at (l, b) ~ (196.2°, +4.8°). Another bright region (R5) at (l, b) ~ (206°, +0.5°) coincides with the Monoceros Loop SNR region. The signal-to-noise ratio for each pixel in these five regions, R1 through R5, was in the range 2.7–10.5.

The C IV emission lines image is compared with those of Hα and X-ray in Figure 2. On the *ROSAT* All-Sky Survey (RASS) X-ray (0.25 keV) image, the FIMS/SPEAR C IV contours, with five levels for the range 8000–16000 LU, are overplotted with thick blue lines, and the Hα contours in the range 8–86 R with thin white lines. The Hα contours show two strong H II regions, NGC 2264 at (l, b) ~ (203.0°, +2.2°)

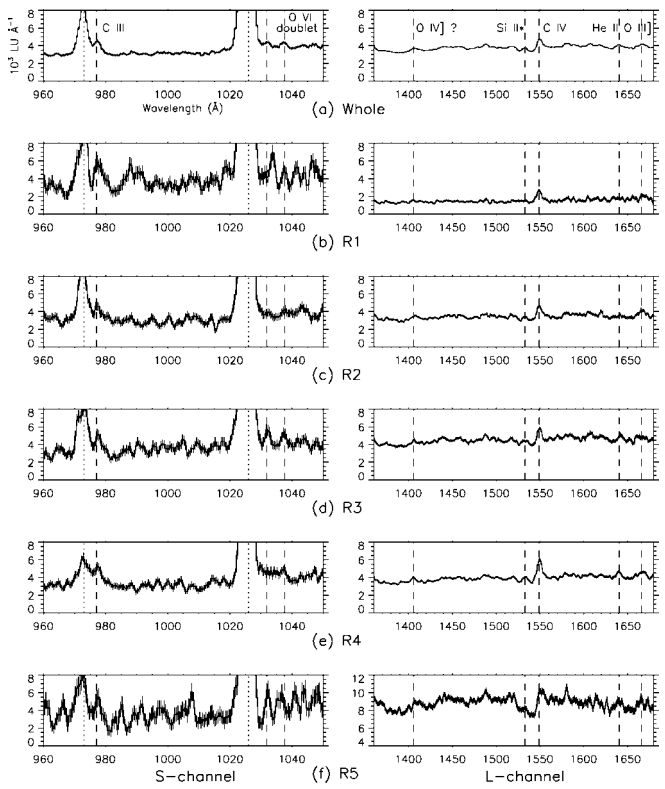

FIG. 3.—FIMS/SPEAR S-channel (*left*) and L-channel (*right*) spectra (with 1 σ error bars) from the whole region and the five subregions indicated in Fig. 1. The spectra were binned with 0.5 and 1 Å for the S- and L-channels, respectively, and smoothed with a boxcar average of 3 bins. The positions of the cosmic lines are indicated by dashed lines. The hydrogen Lyman series (γ 973 Å, β 1026 Å) originating from the geocorona are also marked by dotted lines.

and the Rosette Nebula at $(l, b) \sim (206.3°, -2.1°)$, as well as the Monoceros Loop SNR centered at $(l, b) \sim (205.6°, -0.1°)$. The local peak of the C IV emission at $(l, b) \sim (206°, +0.5°)$ coincides with part of the remnant. In addition, we have identified a faint Hα ring, centered at $(l, b) \sim (191.5°, +5.0°)$, marked with a small black circle of radius 5.7° on the same figure. We call this ring the "Gemini Hα ring." The eastern limb of the Gemini Hα ring fits precisely with the inward distortion of the X-ray emission of the Monogem ring, and the C IV emission peaks along this boundary. Other C IV enhanced regions in the low latitudes are seen to envelop the lower side of the X-ray ring. The positions of the optical filaments found by Weinberger et al. (2006), marked with triangle symbols, coincide with the C IV enhanced edge enveloping the inner X-ray ring. The archival data of Hα and RASS X-ray were adapted from the SkyView virtual observatory (McGlynn et al. 1998).

In Figure 3, we have plotted the spectra for the whole region and the subregions R1 through R5. The detector background was subtracted in these spectra, despite their being quite small: ~0.6% and ~2.6% of the lowest continuum level of R1 for the L- and S-channels, respectively. The spectra were binned with 1 Å for the L-channel and 0.5 Å for the S-channel, and smoothed with a boxcar average of 3 bins. For the whole region in Figure 3, the S-channel spectrum shows definite ionic lines such as C III λ977 and the O VI $\lambda\lambda$1032, 1038 doublet, along with strong geocoronal airglow lines, including the hydrogen Lyman series (γ 973 Å, β 1026 Å). In the L-channel spectrum, Si II* λ1533, He II λ1640, and O III] λ1666 lines can be identified in addition to the prominent C IV $\lambda\lambda$1548, 1550 doublet, which is unresolved due to smoothing.

For each subregion, we fitted the spectrum for the above emission lines to obtain line intensities. Six portions (960–990, 1010–1050, 1525–1540, 1530–1570, 1625–1655, and 1650–1680 Å) were taken from each spectrum and fitted with convolved model lines of Gaussian shape. The centers and the widths of the Gaussian functions were fixed using the calibrated line centers and the FIMS/SPEAR spectral resolutions, respectively. The results are shown in Table 1 for the lines whose intensities were determined with >3 σ significance. While Table 1 indicates that C IV is the most intense in all regions R1 through R5, we also note that no enhanced features were found in other regions of Figure 1 for any of the above-mentioned FUV lines. The C III line is detected at >3 σ significance in all regions R1 through R5, but O VI doublet lines are detected only in R3 and R4. Si II* and He II lines are detected only in R4, and the O III] line only in R2 and R4. We can estimate the C IV luminosity of the whole Monogem ring using the value 7.1×10^3 LU in Table 1. The result is 15.6×10^{34} ergs s^{-1} with a distance of 300 pc to the target, without correction for interstellar extinction. While little is known about the foreground extinction along the line of sight toward the Monogem ring, we do not expect it to significantly affect our estimation, since the neutral hydrogen column density to the target is small ($N_{\rm H} \sim 5.0 \times 10^{19}$ cm^{-2}; Plucinsky et al. 1996). The C IV luminosity is ~3–5 times less than that of the Cygnus loop, 44.7×10^{34} ergs s^{-1} (Seon et al. 2006) or the Vela, 80.0×10^{34} ergs s^{-1} (Nishikida et al. 2006).

4. DISCUSSION

The observed C IV emission features in the low-latitude regions (R2 through R5) agree well with the picture that expansion of the Monogem SNR is blocked by a relatively dense medium toward the Galactic plane in the low-latitude region (Hnatyk & Petruk 1999). In particular, C IV appears the brightest where the expanding blast wave interacts with the Gemini Hα ring (R4). In addition, the X-ray image in Figure 2 shows that hot gas is extended in the high-latitude region where C IV emission is not seen, beyond the circle of radius 9.2° centered

TABLE 1
FUV LINE INTENSITIES

Species	Whole	R1	R2	R3	R4	R5
C III λ977	4.9 ± 0.4	6.6 ± 2.1	4.3 ± 1.3	6.1 ± 1.5	7.2 ± 1.2	8.2 ± 2.4
O VI $\lambda\lambda$1032, 1038	4.0 ± 0.5	...	(4.1 ± 1.6)	7.2 ± 2.0	5.6 ± 1.5	...
Si II* λ1533	1.9 ± 0.2	...	(1.8 ± 0.7)	(2.0 ± 0.9)	2.7 ± 0.6	...
C IV $\lambda\lambda$1548, 1550	7.1 ± 0.2	8.7 ± 0.9	9.3 ± 0.8	9.2 ± 0.9	14.3 ± 0.7	10.3 ± 1.9
He II λ1640	2.3 ± 0.3	...	...	(2.9 ± 1.1)	4.2 ± 0.8	(5.2 ± 2.2)
O III] λ1666	2.5 ± 0.3	...	4.9 ± 1.0	...	3.9 ± 0.9	(5.8 ± 2.4)

NOTE.—Line intensities are in units of 10^3 LU. R1 through R5 correspond to regions shown in Fig. 1. All intensities were determined with >3 σ significance except for those in parentheses, which were determined with >2 σ significance.

at the position of pulsar PSR B0656+14. The morphology appears to support the association of the remnant with the pulsar, as conjectured by Thorsett et al. (2003). The C IV enhancement feature in the high-latitude region (R1) is likely due to the interaction of the blast wave with an isolated cloud. This is supported by the X-ray emission, which is fainter in the middle of R1 but bright around the edges, as can be seen in Figure 2.

Each of the FUV emission lines identified in Figure 3 corresponds to its own characteristic ionization energy: 8.1 eV for Si II*, 24.4 eV for C III, 24.6 eV for He II, 35.2 eV for O III], 48 eV for C IV, and 114 eV for O VI. Hence, the inner C IV enhancement region, R3, where O VI doublets are more prominent, is expected to have a higher temperature than region R4, where O VI doublets are weak, but C III, Si II*, He II, and O III] lines with lower ionization energies are prominent. As discussed above, R4 is the region where the Monogem ring interacts most with its cooler neighboring medium. The L-channel spectrum of R5 has a much higher continuum level than those of other regions, which is undoubtedly caused by the direct and dust-scattered stellar background. Futhermore, a spectral profile around C IV resembles those of P-Cygni type stars, implying that the contribution from bright O- and B-type stars still remains. However, since this region includes part of the Monoceros Loop SNR, as can be seen in Figure 2, we believe the local peak of C IV around (l, b) ~ (206°, +0.5°) is real, and at least some portion of the C IV emission detected in R5 originates from the diffuse hot gas of the Monoceros Loop SNR.

5. CONCLUSIONS

We have presented the results of FUV observations made for the Monogem ring using the new data set of FIMS/SPEAR. We detected important ionic emission lines, such as C III, O VI, Si II*, C IV, He II, and O III], from various regions of the target. A map constructed from C IV emission lines showed clear evidence of interaction with the ambient medium. The C IV enhancement features in the low-latitude region were located at the envelope of the soft X-ray (0.25 keV) ring, indicating interaction with a relatively dense medium toward the Galactic plane. On one side of the Monogem ring, a prominent C IV peak was seen at the boundary of the newly found Hα ring (Gemini Hα ring), centered at (l, b) ~ (191.5°, +5.0°), which is in direct contact with the hot gas, distorting the morphology of the X-ray ring. On the other hand, the hot gas was seen to expand freely in the high-latitude region without significant interaction with the ambient medium, producing no significant large-scale C IV emission features except a small local enhancement. The morphology appears to be consistent with the conjecture that the pulsar PSR B0656+14 is a progenitor of the SNR.

FIMS/SPEAR is a joint project of the Korea Advanced Institute of Science and Technology, the Korea Astronomy and Space Science Institute, and the University of California at Berkeley, funded by the Korean Ministry of Science and Technology and the National Aeronautics and Space Administration (NASA) Grant NAG5-5355. We used NASA's SkyView facility (http://skyview.gsfc.nasa.gov).

REFERENCES

Brisken, W. F., Thorsett, S. E., Golden, A., & Goss, W. M. 2003, ApJ, 593, L89
Bunner, A. N., Coleman, P. L., Kraushaar, W. L., & McCammon, D. 1971, ApJ, 167, L3
Bunner, A. N., Coleman, P. L., Kraushaar, W. L., McCammon, D., & Williamson, F. O. 1973, ApJ, 179, 781
Davidsen, A., Shulman, S., Fritz, G., Meekins, J. F., Henry, R. C., & Friedman, H. 1972, ApJ, 177, 629
Edelstein, J., et al. 2006a, ApJ, 644, L153
———. 2006b, ApJ, 644, L159
Górski, K. M., et al. 2005, ApJ, 622, 759
Hnatyk, B., & Petruk, O. 1999, A&A, 344, 295
Long, K. S., Patterson, J. R., Moore, W. E., & Garmire, G. P. 1977, ApJ, 212, 427
McGlynn, T., Scollick, K., & White, N. 1998, in IAU Symp. 179, New Horizons from Multi-Wavelength Sky Surveys, ed. B. J. McLean et al. (Dordrecht: Kluwer), 465
Nishikida, K., et al. 2006, ApJ, 644, L171
Nousek, J. A., Cowie, L. L., Hu, E., Lindblad, C. J., & Garmire, G. P. 1981, ApJ, 248, 152
Plucinsky, P. P., Snowden, S. L., Aschenbach, B., Egger, R., Edgar, R. J., & McCammon, D. 1996, ApJ, 463, 224
Reimers, D., & Wendker, H. J. 1984, A&A, 131, 375
Seon, K.-I. 2006, J. Korean Phys. Soc., 48, L331
Seon, K.-I., et al. 2006, ApJ, 644, L175
Slavin, J. D., & Cox, D. P. 1992, ApJ, 392, 131
Thorsett, S. E., Benjamin, R. A., Brisken, W. F., Golden, A., & Goss, W. M. 2003, ApJ, 592, L71
Vallée, J. P., Broten, N. W., & MacLeod, J. M. 1984, A&A, 134, 199
Weinberger, R., Temporin, S., & Stecklum, B. 2006, A&A, 448, 1095
Yentis, D. J., Novick, R., & Vanden Bout, P. 1972, ApJ, 177, 375